

Microstructural Characterization of Equiatomic CrFeNbNiV Alloy

A. Saikumaran¹ · R. Mythili²  · S. Saroja³ · V. Srihari⁴

Received: 3 July 2018 / Accepted: 4 November 2018 / Published online: 1 December 2018
© The Indian Institute of Metals - IIM 2018

Abstract This paper presents the results of an experimental study to investigate the structural and microchemical characteristics of an equiatomic CrFeNbNiV alloy. XRD analysis of CrFeNbNiV alloy, revealed a predominant NbCrNi type HCP Laves phase conjoined with two minor tetragonal and BCC phases. Detailed microstructural investigations using electron microscopy techniques also substantiated the presence of the above mentioned phases. The structure of Laves phase in this alloy is determined ab initio for the first time using Precession Electron Diffraction technique which was in agreement with the Rietveld analysis of XRD pattern. The formation of intermetallic Laves phase was understood based on theoretical phase stability and average *d*-orbital energy level $\bar{M}d$ value calculations. The alloy in the ‘as cast’ condition exhibited a very high value of hardness (~ 1500 Hv). No change in the microstructure and hardness was observed on annealing at high temperatures even up to 1373 K (1100 °C).

Keywords High entropy alloy · Precession electron diffraction · Automated diffraction tomography · Microstructure · Laves phase · Phase stability

✉ R. Mythili
rm@igcar.gov.in

¹ Indira Gandhi Centre for Atomic Research, Homi Bhabha National Institute, Kalpakkam, India

² Materials Characterization Group, Metallurgy and Materials Group, IGCAR, Kalpakkam, India

³ IGCAR, HBNI, Kalpakkam 603102, India

⁴ High Pressure & Synchrotron Radiation Physics Division, Bhabha Atomic Research Centre, Mumbai, India

1 Introduction

There has been an intense research on Multi-Principal Elemental Alloys (MPEAs) in the recent years due to their unique microstructure and properties. J. W. Yeh classified these alloys consisting of alloying elements in equiatomic or near equiatomic concentration as High Entropy Alloys (HEAs) [1]. It is believed that, significantly higher entropy of mixing from such complex compositions could simplify the structure and microstructure, and ultimately lead to a single solid solution phase which imparts attractive properties to the alloys [2–6]. Most of the HEAs reported usually comprise of FCC [7–11] or BCC [12–15] solid solution. The former class contains Al, Co, Cr, Cu, Fe and Ni with small additions of Mn, Mo and Ti, while the latter group of alloys contain refractory elements such as Mo, Nb, Ta, W, Ti, Hf, V and Zr, with addition of Fe, Cr, Cu and Al. However, since their invention, several investigations on the microstructure of most of these MPEAs have shown the presence of nanoscale precipitates/dispersoids, intermetallic phases, topological close packed phases, dendritic and inter-dendritic structures, and coexistence of amorphous phases in addition to the matrix phase [1, 16–23], which clearly suggests that several HEAs form multiphase structures rather than single phase solid solution.

The aim of the present work is to study the nature of phases that would evolve and their stability on addition of an FCC element (Ni) to a base of four BCC elements (Fe, Cr, Nb, V) in an equiatomic composition. The resultant microstructural characteristics and its influence on hardness have also been studied. Ferritic steels, due to their excellent void swelling resistance are candidate structural materials for future GEN-IV nuclear reactors, though the high temperature mechanical properties need improvement

[24–27]. Therefore, the choice of components of this alloy has been made based on the major alloying elements in ferritic steels. Hence, this study reports the microstructural characteristics at ambient and high temperatures of an equiatomic CrFeNbNiV alloy, through extensive electron microscopy investigations.

2 Materials and Methods

Equiatomic CrFeNiNbV alloy was synthesized by vacuum arc melting technique from high purity raw materials of Fe, Cr, V, Nb and Ni using a tungsten electrode tri-arc furnace with water cooled copper hearth under high purity (99.99%) argon atmosphere. The alloys were remelted three to four times and also flipped between two melting processes to obtain chemical homogeneity due to the large difference in melting points and densities of the raw materials.

The alloy was subjected to aging treatments at different temperatures ranging from 873 K to 1373 K (600 to 1100 °C) for 4 h followed by rapid quenching in liquid nitrogen, to avoid any phase transformations during cooling. Aging treatments were carried out in vacuum $\sim 10^{-6}$ mbar in a high vacuum furnace, in order to avoid oxidation of the alloy at high temperatures. Phase constitution of the alloy was examined by X-Ray Diffraction (XRD) analysis in transmission geometry using the in house Micro XRD setup (GENIX 3D supplied by Xenocs, France) with Mo target with a wavelength of 0.711 Å and a MAR345 IP detector. In-depth analysis was carried out by Synchrotron XRD experiments using Angle Dispersive X-Ray Diffraction (ADXRD) beamline (BL-11) of photon energies 20 keV ($\lambda = 0.694722$ Å) and 28 keV ($\lambda = 0.44092$ Å), photon flux ($> 10^9$ photons/s) and beam size $300 \times 300 \mu\text{m}^2$ at the Indian Synchrotron Source (Indus 2) at Raja Ramana Centre for Advanced Technology, Indore.

The sample surfaces were sequentially polished down to the 0.3 μm grit alumina suspension furnish, and then chemically etched using a solution containing 95% nitric acid and 5% hydrofluoric acid for microstructural analysis. Preliminary analysis was carried out using Scanning Electron Microscopy (SEM, Helios Nanolab 600i Dual beam FESEM) equipped with energy dispersive X-ray (EDX) spectrometer. Specimen for Transmission Electron Microscopy (TEM) were prepared by mechanically grinding up to 150 μm thickness, from which disks of 3 mm diameter were punched out and further reduced to 50 μm thickness using a tripod polisher. Final thinning of specimen was carried out by ion milling using a Technoorg Linda IV4/H ion miller using argon ions (Ar^+). Site specific TEM specimen were prepared by Focused Ion Beam (FIB) technique (attached to Helios 600i FESEM).

The samples were welded to an omniprobe Cu grid and further thinned to obtain electron transparency. TEM studies were carried out using Philips CM200 Analytical Transmission Electron Microscope (ATEM) equipped with Oxford X-Max SDD detector for microchemical analysis.

Precession Electron Diffraction (PED) [28] experiments for ab initio crystal structure determination were carried out using a PED system from Nanomegas SPRL, Belgium in the Philips CM200 ATEM. A series of electron diffraction patterns were collected from -15° to $+15^\circ$ with an interval of 1° from the region of interest using a single tilt holder, and beam precession angle of 1.04° and 50 μm C2 condenser aperture. The collected diffraction patterns were processed using the 3D-Automated Diffraction Tomography (ADT) analysis, which includes various steps like stacking of the diffraction patterns, background correction, centering of patterns, finding and refining the tilt axis, reconstruction of volume data and finding the unit cell parameters by optimizing clustering parameters. Further details of the software can be found elsewhere [29, 30]. Vickers hardness measurements were carried out using Leitz Miniload -2 micro hardness tester at a constant load of 100 g and a dwell time of 10 s.

3 Results and Discussion

This section presents the results on the prediction of phases in the equiatomic CrFeNbNiV alloy using empirical calculations and the structural analysis in the ‘as cast’ and aged conditions. The measured value of hardness is correlated with the resultant microstructures.

3.1 Theoretical Phase Stability Calculations

Limited literature is available on the nature of phases in the aforementioned composition. Hence, type of phase that forms in these alloys is predicted, using the well known empirical parameters of atomic size difference (δ), Electronegativity difference ($\Delta\chi$), Valence Electron Concentration (VEC), Enthalpy (ΔH_{mix}) and entropy of mixing (ΔS_{mix}) [31–37]. The values of atomic radius, Pauling’s electronegativity, VEC and melting temperature (T_m) [31] of individual elements as well as values of binary enthalpies of mixing (Table 1) [38] are obtained from literature.

The calculated empirical parameters and predicted phases for the equiatomic CrFeNbNiV system are shown in Table 2. It has been reported that BCC solution forms when the value of VEC is less than 6.87 [31]. Hence, it can be inferred from Table 2, that equiatomic CrFeNbNiV system forms a BCC solid solution (SS) phase. In addition, value of VEC of the alloy also indicates the possibility of formation of intermetallic phases.

Table 1 Binary enthalpies

Binary system	Fe–Cr	Fe–V	Fe–Nb	Fe–Ni	Cr–V	Cr–Nb	Cr–Ni	V–Nb	V–Ni	Nb–Ni
ΔH_{mix} (kJ/mol)	– 1	– 7	– 16	– 2	– 2	– 7	– 7	– 1	– 18	– 30

Table 2 Theoretical phase stability calculation of equiatomic CrFeNbNiV alloy

Alloy	δ	ΔH_{mix} (kJ/mol)	ΔS_{mix} (J/K mol)	$\Delta\chi$	VEC	Ω	Phase predicted
CrFeVNBnNi	0.04	– 10.56	13.8	0.26	6.84	1.25	BCC SS

3.2 Phase Identification in as Cast Alloy

Figure 1 shows the XRD spectrum of the as cast CrFeNbNiV alloy obtained using synchrotron radiation. Analysis of the spectrum indicates that most of the peaks match for CrNiNb type Hexagonal Close Packed (HCP) Laves phase (marked with *), suggesting that the Laves phase is the major phase. Few other peaks are also observed in Fig. 1. Combined with electron diffraction pattern analysis given in the forthcoming section, they have been identified to belong to $V_{0.7}Ni_{0.3}$ type intermetallic tetragonal sigma phase (marked with #) with lattice parameters of $a = 0.898$ nm and $c = 0.464$ nm and a BCC phase (marked with \$) with a lattice parameter of $a = 0.327$ nm.

3.3 Microstructural and Microchemical Characterisation

Figure 2a shows the Secondary Electron (SE) image of as cast CrFeNbNiV alloy, which shows regions of different

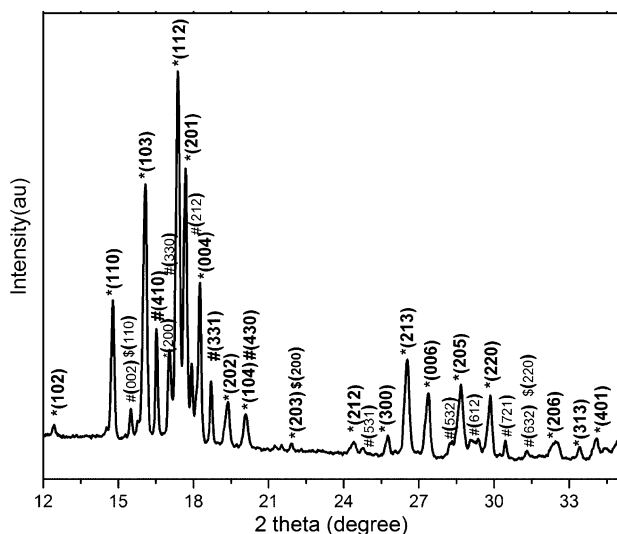


Fig. 1 XRD spectrum of as cast CrFeNbNiV alloy using Synchrotron radiation showing the presence of different phases

contrasts. Microchemical analysis by Energy dispersive X-Ray Spectroscopy (EDX point analysis) (Fig. 2b, c) from different locations of the specimen shows that there are two types of regions present in this alloy namely (1) Nb- rich and (2) Nb- lean V-Cr rich regions, suggesting the presence of two phases. However, it is observed that these two phases, show a small amount of solubility for other alloying elements also. The magnified image of the region indicated in Fig. 2a is given in Fig. 2d which clearly shows the two compositionally different phases. EDX elemental maps given in Fig. 3a–e also confirm the presence of two phases. It can be clearly seen from Fig. 3f that the Nb lean phase is rich in V and Cr.

Figure 4a shows the TEM bright field image of as cast CrFeNbNiV alloy along with the SAD pattern (Fig. 4b) taken from region circled in Fig. 4a. Analysis of the SAD pattern combined with composition from EDX analysis (Fig. 4c) also confirms the presence of Nb rich hcp Laves phase along $[-5\ 10\ 6]$ zone axis (ZA).

TEM bright field image of the alloy from another location is given in Fig. 5a. EDX spectra from regions 1 and 2 (circled in 5(a)) are given in Fig. 5b, which shows that the composition of these regions is lean w.r.t Nb, but richer in V, Cr, without any significant difference. In Fig. 4c and 5b, Cu peak is intense probably due to contribution from Cu omniprobe grid. Figure 5c, d shows the SAD patterns from regions 1 and 2 respectively (circled in (a)). Analysis of these SAD patterns show that these V-Cr rich precipitates in region 1 of Fig. 5a corresponds to sigma phase of $V_{0.7}Ni_{0.3}$ type and a tetragonal structure (Fig. 5c) with $a = 0.89$ nm and $c = 0.46$ nm. Analysis of SAD pattern from region 2 of Fig. 5a corresponds to a BCC structure (Fig. 5d) with $a = 0.32$ nm, which is consistent with the XRD observations. Though some of the d-spacings of BCC phase match with that of the tetragonal phases, the systematic analysis of the reflections in Fig. 5d clearly establishes the presence of BCC phase. SAD analysis has been carried out on various regions with similar compositions to confirm the presence of the BCC and

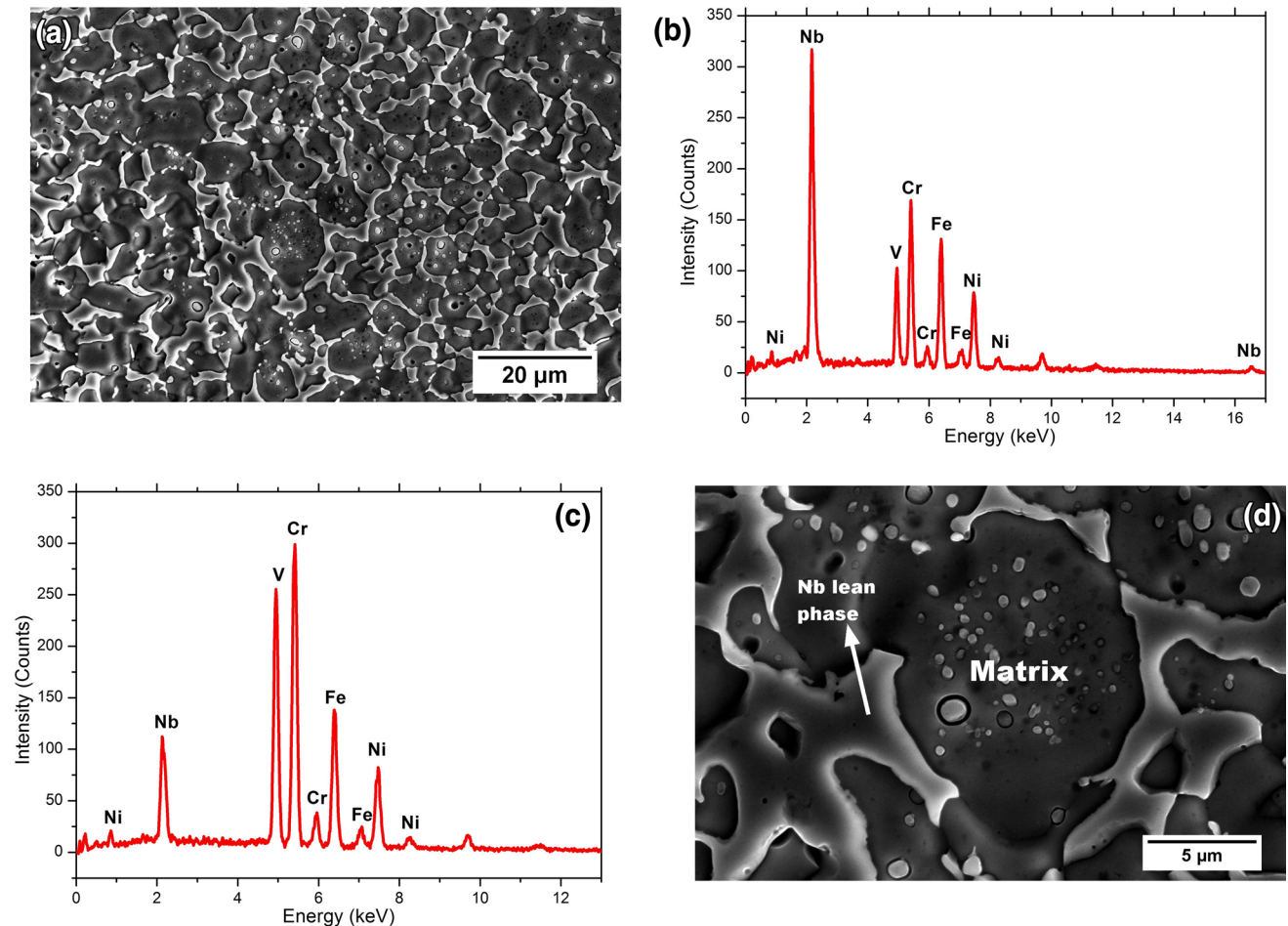


Fig. 2 a SE Micrograph of as cast CrFeNbNiV alloy showing a two phase structure; EDX spectra of **b** Nb rich phase **c** Nb lean phase **d** Magnified image of 2(a)

tetragonal phases. Figure 5 e, f show the DF images of tetragonal phase with (200) reflection and BCC with (-100) reflections respectively. To sum up, it is identified that in as cast CrFeNbNiV alloy, major phase is HCP Laves phase with small amounts of BCC and tetragonal phases.

3.4 Structural Analysis of Laves Phase

Precession electron diffraction (PED) combined with 3D Automated Diffraction Tomography (ADT) has been carried out in TEM for ab initio crystal structure determination of Nb rich Laves phase. For the PED–ADT analysis, a suitable region from the Laves phase is selected and prepared by FIB technique. A stack of the tilt series of diffraction patterns are collected from Laves phase, a few of which are shown in Fig. 6a–f.

After centering and rotation of the tilt series to the appropriate tilt axis from the stereographic projection of the tilt series, strong reflections or peaks in the volumetric

data are identified and difference vectors for all peak positions identified in the experimental data are calculated [30]. The 3 shortest and the most repeated non coplanar vectors in the difference vector space correspond to the unit-cell vectors, which are obtained after excluding the noisy data close around the central beam. The sphere of exclusion in the diffraction data set is shown in Fig. 7 and the projection of the reciprocal lattice along the three directions is shown in Fig. 8. Using this procedure, the unit cell parameters of Laves phase have been determined to be as follows: $a = 0.47629$ nm, $c = 0.79249$ nm; $\alpha = 90^\circ$, $\beta = 90^\circ$, and $\gamma = 120^\circ$.

In order to confirm the above analysis, Rietveld refinement of the synchrotron XRD spectrum was carried out with the inputs obtained from ADT analysis. The Rietveld refined spectrum is shown in Fig. 9 which confirms that the unit cell parameters determined from ADT and Rietveld analyses are in agreement.

Fig. 3 Elemental X-ray maps of as cast CrFeNbNiV alloy showing the distribution of **a** Nb **b** V **c** Cr **d** Fe **e** Ni **f** combined X-ray map showing Nb rich and Nb lean, Cr,V rich regions

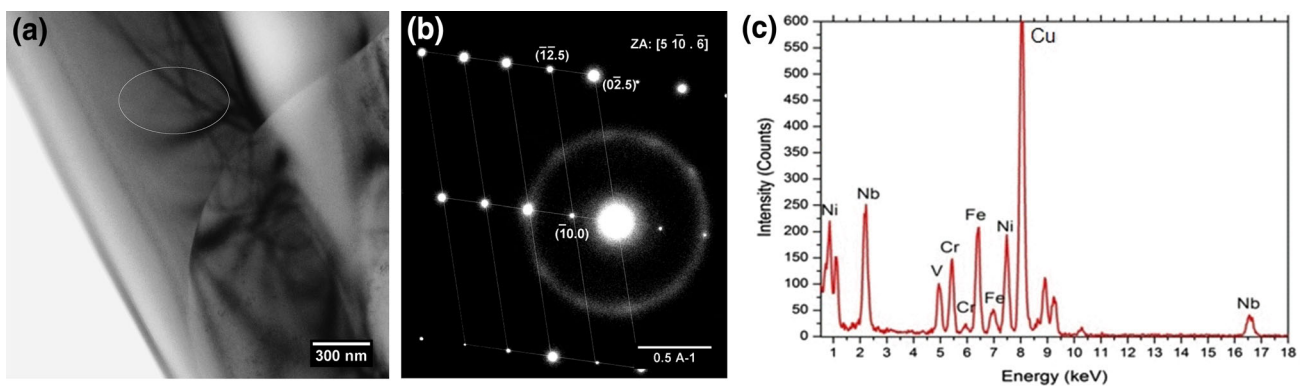
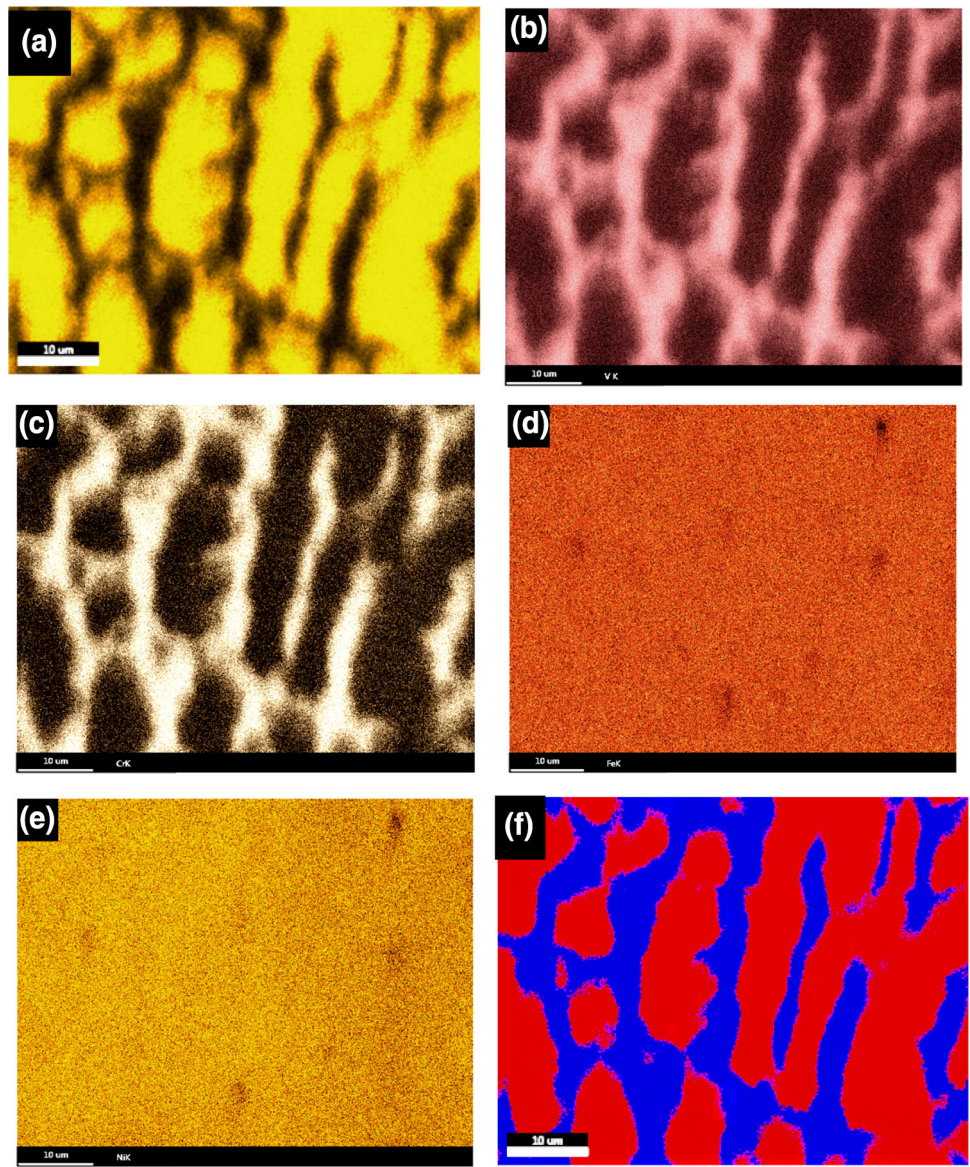


Fig. 4 **a**TEM BF image as cast CrFeNbNiV alloy; **b** SAD pattern from region circled in **a** confirming HCP Laves phase along $[-5\ 10\ 6]$ zone axis; **c** EDX Spectrum from circled region in **a** showing the enrichment of Nb

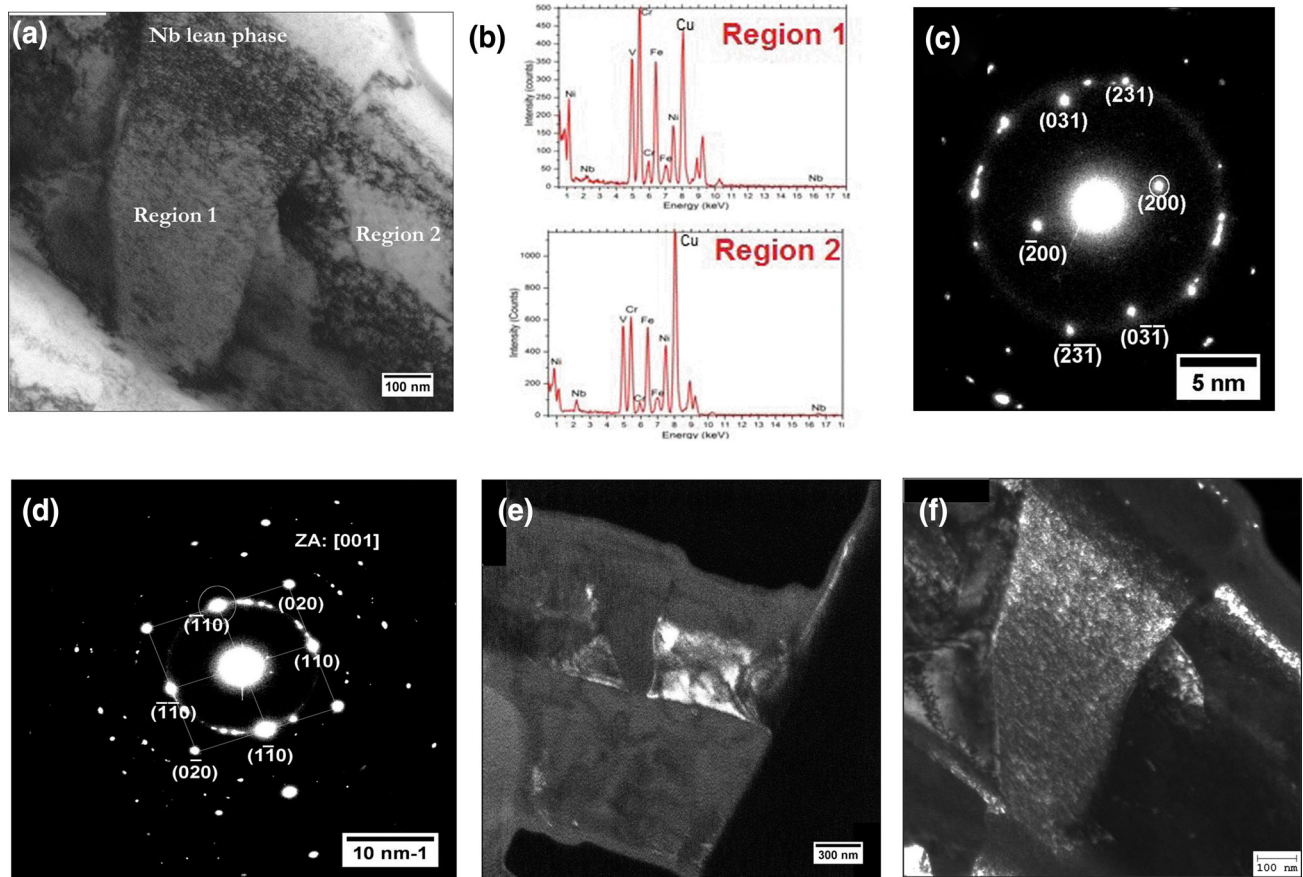


Fig. 5 **a** BF image of as cast CrFeNbNiV alloy; **b** EDX spectra from regions 1,2 showing enrichment of V, Cr; **c**, **d** SAD patterns from regions 1,2 in **a** confirming presence of tetragonal and BCC phases along [0–13] and [001] zone axis respectively; **e**, **f** DF images of tetragonal phase with (200) and BCC phase with $(-1\ 1\ 0)$ reflection respectively

3.5 Effect of High Temperature Exposure on Microstructure

Figure 10 shows the XRD patterns of the CrFeNbNiV alloy heat treated in the temperature range of 873 K to 1373 K. It is evident that there is no additional peak or significant change in peak position in comparison to the as cast alloy, suggesting negligible change in phase constitution.

Analysis of SEM images shown in Fig. 11a–c also did not indicate any significant change in microstructure of the alloy after high temperature exposure.

Figure 12a, b show the TEM bright field images of the alloy heat treated at 1100 °C. The SAD patterns corresponding to Laves phase (from Fig. 12a), tetragonal (from Fig. 12b and BCC (from Fig. 12a)) are shown in Fig. 8 c–e respectively along $[-11.0]$, $[11-5]$ and $[-110]$ zone axis respectively, similar to the as cast alloy. The corresponding DF images for the tetragonal and BCC phases are shown in Fig. 12f and g respectively. These observations suggest microstructural stability at high temperatures. Comparison of activation energy for diffusion in the constituent binary

alloys [39] at temperatures around 1373 K show that, Nb has the highest activation energy in the range of 330–360 kJ mol⁻¹, while for the other combinations, the activation energy is in the range of 265–295 kJ mol⁻¹. This suggests that Nb is the slowest diffusing species, which is responsible for the microstructural stability at this high temperature.

3.6 Rationale Behind Formation of HCP Laves and Tetragonal Sigma Phases

The above experimental evidences clearly show the formation of the intermetallic HCP Laves phase as a major phase, which is in contradiction to the empirical calculations, though the VEC value of 6.84, suggests a possibility of formation of intermetallic phases like sigma and Laves phases. For the formation of topological close packed phases in HEAs, the average energy of *d* orbital, \overline{Md} has been calculated for this alloy using the following equation as proposed by Morinaga, et al. [40] for Ni based super alloys.

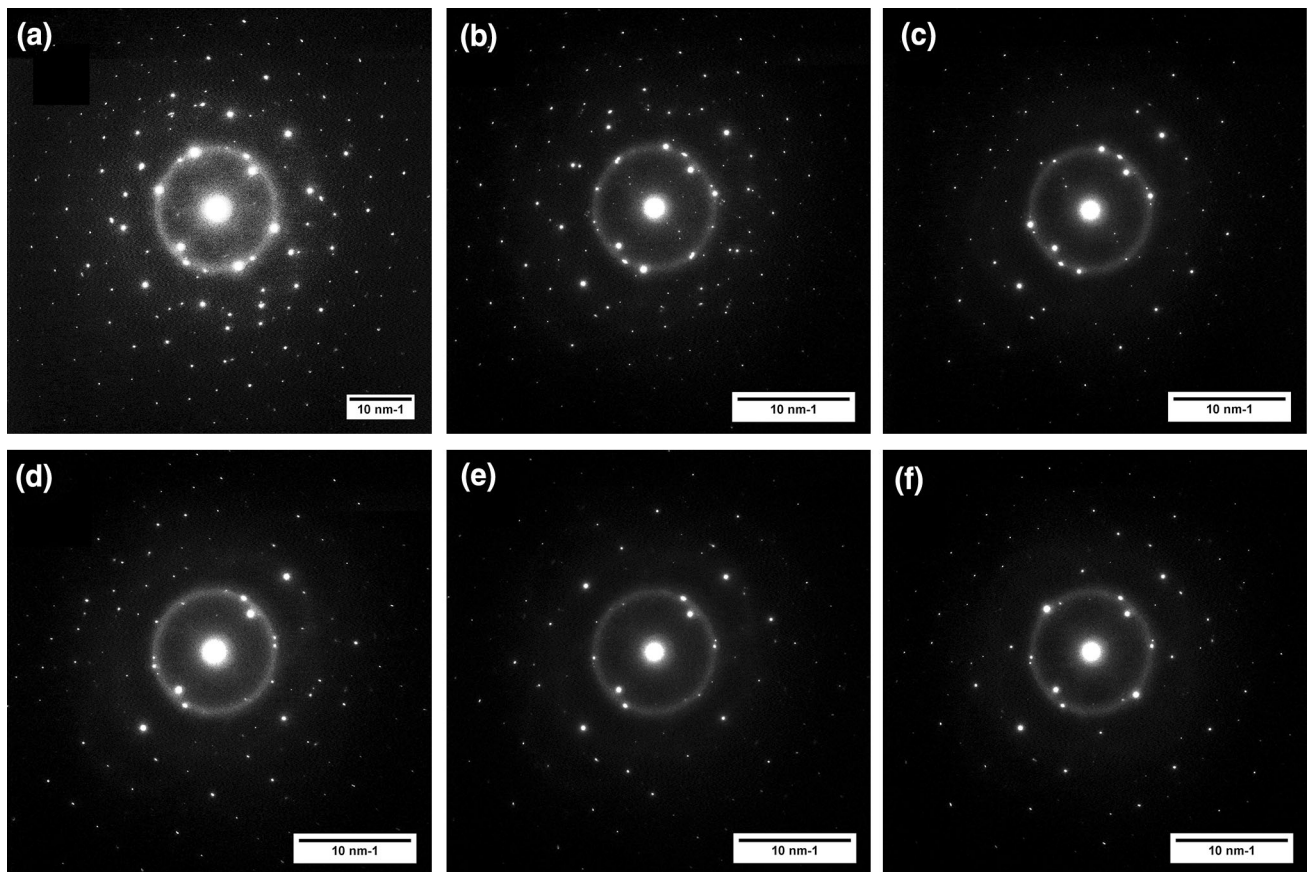


Fig. 6 Series (sample) of electron diffraction patterns collected from Laves phase of equiatomic CrFeNbNiV alloy at different tilt angles **a** – 2° **b** 6° **c** 3° **d** 7° **e** 10° **f** 14°

$$\overline{\text{Md}} = \sum_{i=1}^n C_i(\text{Md})_i \quad (1)$$

These metal-d levels (Md) correlate with electronegativity and atomic radius and the individual values of Md for various transition metals obtained from ref [40] are listed in Table 3. Md value calculated for each element is the average of e_g and t_{2g} values. Morinaga, et al. [40] suggested that when the Md becomes larger than a certain critical value, the instability of γ phase takes place in Ni based superalloys and the second phase precipitation occurs in a γ matrix. In other words, Md parameter determines the solubility limit of γ matrix. This concept of Md was extended to HEAs by Yiping Lu et al. [41] who did numerous $\overline{\text{Md}}$ calculations (using above equation) on a number of HEA systems assuming FCC Ni_3Al structure for all HEAs of their study, and came to a conclusion that the threshold value of $\overline{\text{Md}}$ for the formation of intermetallic laves phases was 1.09. In the present study, $\overline{\text{Md}}$ for the current alloy has been calculated and is found to be 1.46, which is well above the threshold value for the formation

of close packed intermetallic phases. Hence, it is understood that this $\overline{\text{Md}}$ parameter dictates the formation of HCP Laves phase and tetragonal sigma phase in this alloy.

Moreover, earlier microstructural investigations on Nb containing HEAs have also elucidated the presence of Laves phases. For instance, it has been reported by Y Zhang et al. [42] that the presence of Nb decreases the stability of the solid solution phase, which promotes the formation of ordered Laves phase. They have observed that as the Nb content increases, the atomic size difference increases and Ω value decreases, which implies that the stability of the solid-solution phase decreases with Nb addition; thus, ordered Laves phase appears in Nb containing alloys. Feng He et al. [43] have reported the presence of a $(\text{CrFe})(\text{CoNi})\text{Nb}$ intermetallics in CoCrFeNiNb_x ($x = 0.1, 0.25, 0.5$ and 0.8) system, while Zhang et al. [42] have reported a $(\text{CoCr})_2\text{Nb}$ type HCP laves phase in the CoCrFeNiAlNb_x ($x = 0, 0.1, 0.25, 0.5$, and 0.75) system. Similarly Li Jiang et al. [44] have studied the microstructure of $\text{CoFeNi}_2\text{V}_{0.5}\text{Nb}_{0.75}$ alloy and reported the presence

Fig. 7 Reconstructed 3D volume data from the 2D tilt series

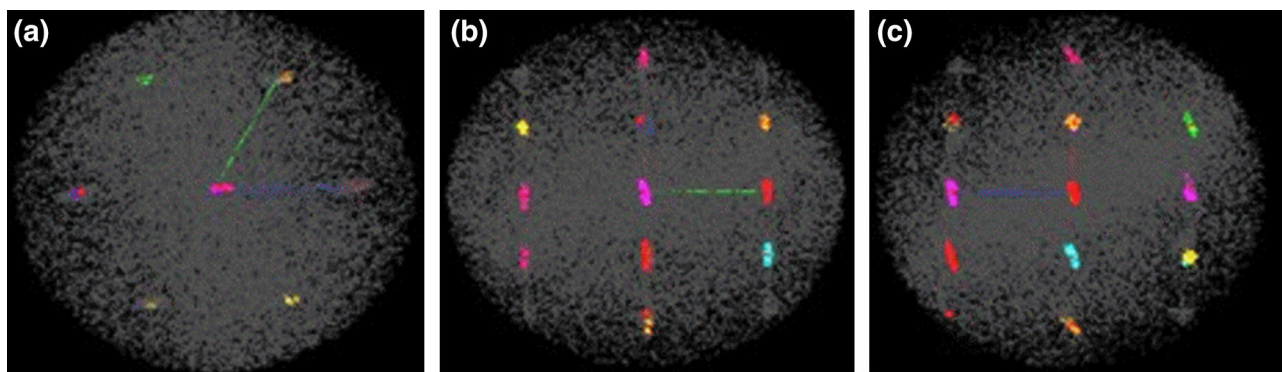
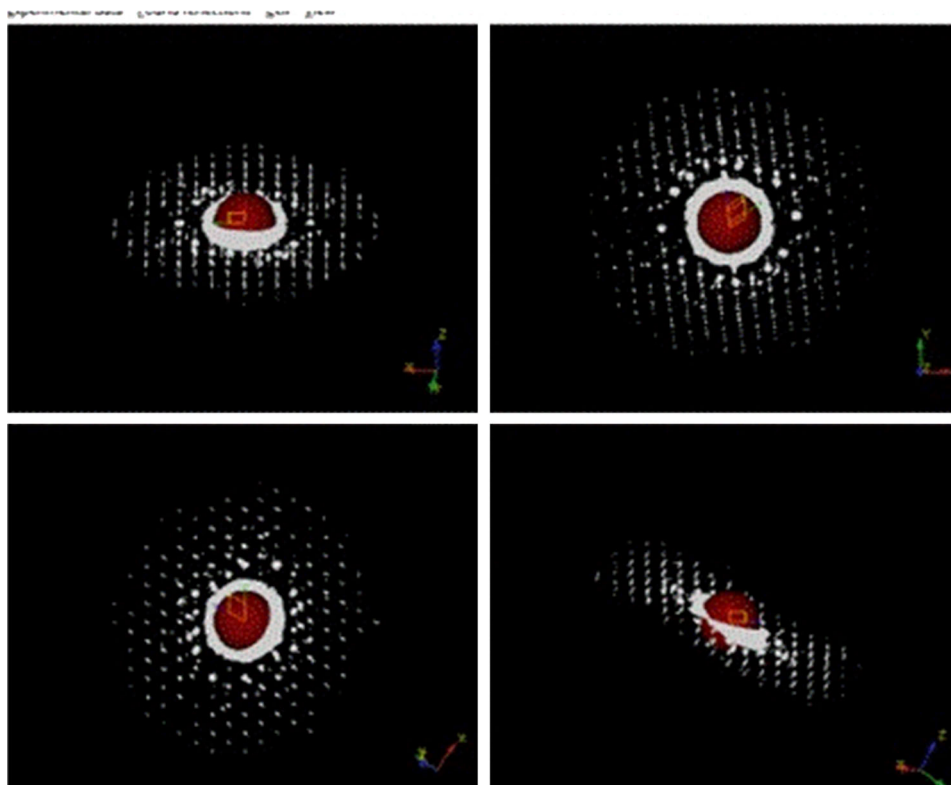


Fig. 8 Projection of the reciprocal lattice along **a** c direction **b** a direction **c** a direction

of Fe_2Nb type HCP Laves phase and NbNi_4 intermetallics in the microstructure.

3.7 Effect of Temperature on Hardness

The hardness of the initial as cast alloy has been found to be very high (1500 ± 10 Hv), which can be attributed to the formation of brittle Nb rich Laves phase. Exposure to 1373 K (1100 °C), have not shown any reduction in hardness, which is similar to the as cast condition. Hence, it can be inferred that this alloy shows an excellent high temperature stability and resistance to anneal softening, which are the unique properties of HEAs.

4 Conclusions

Equiatomic CrFeNbNiV HEA has been synthesized through conventional vacuum arc melting technique. Detailed microstructural and microchemical investigations has revealed the existence of multiple phases in this alloy and following are the salient results obtained from this study.

- Theoretical phase stability calculations suggested the formation of a bcc solid solution and an intermetallic phase due to high value of VEC.
- Presence of Nb rich NbCrNi type Laves phase as major phase along with two minor tetragonal and BCC phases was identified.

Fig. 9 Rietveld refined spectrum of as cast equiatomic CrFeNbNiV alloy

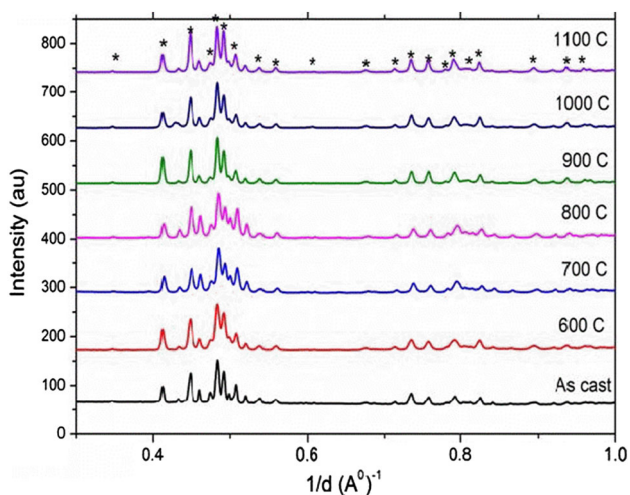
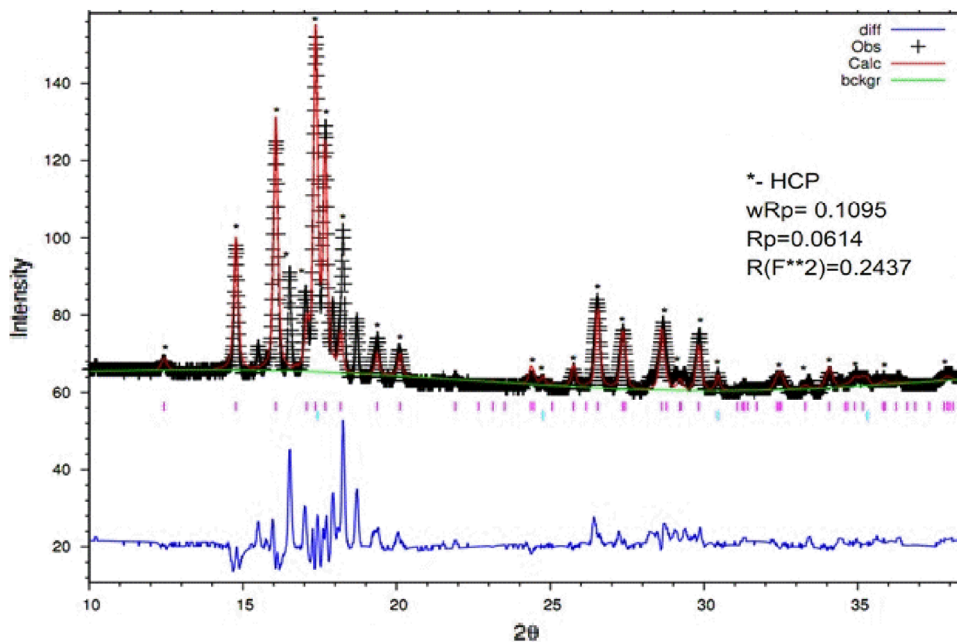


Fig. 10 XRD spectra of CrFeNbNiV alloy aged at different temperatures

- c. The high hardness of the alloy could be attributed to the formation of intermetallics Laves phase.
- d. The unit cell parameters of Laves phase were determined for the first time by precession assisted Automated Diffraction Tomography in TEM and confirmed by X-ray Rietveld analysis.
- e. Comparison of activation energy for diffusion in the constituent binary alloys showed that Nb was the slowest diffusing species, if extended to this alloy offered an explanation for the observed high temperature microstructural stability.
- f. The formation of intermetallic phases like Laves phase and Sigma phase in the alloy could be explained based on the synergistic effect of high average value of *d*-orbital energy level and high atomic size of Nb.

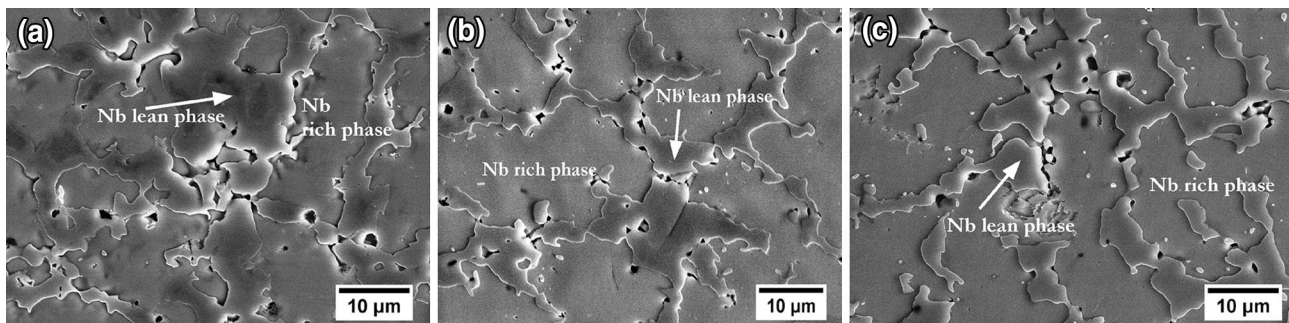


Fig. 11 SEM micrographs of CrFeNbNiV alloy aged at **a** 600 °C **b** 900 °C **c** 1100 °C showing the presence of both Nb rich Laves and V, Cr phases at all temperatures

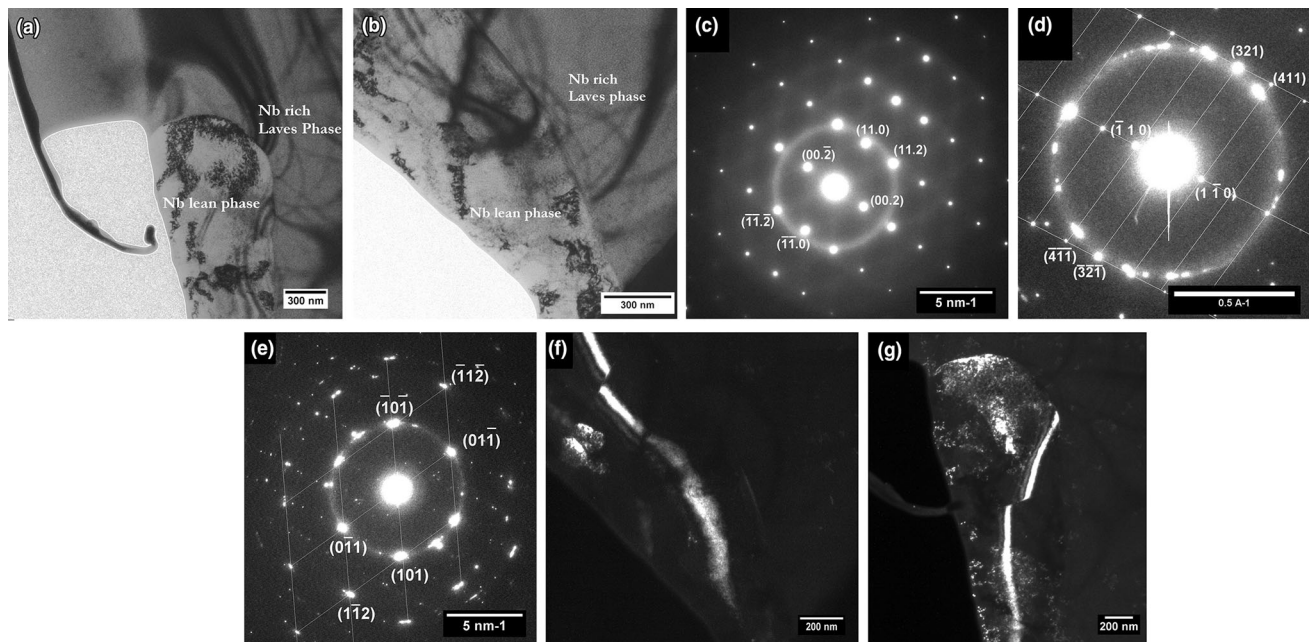


Fig. 12 a & b BF images of CrFeNbNiV alloy aged at 1100 °C; SAD patterns of c HCP Laves phase along [-11.0] ZA d Tetragonal V-Cr rich phase along [11-5] ZA e BCC V-Cr rich phase along [-111] ZA f DF image of Tetragonal V-Cr rich precipitates with reflection circled in Fig. 8d; g DF image of BCC V-Cr rich precipitates with (-10-1) reflection

Table 3 Md value for individual elements

Element	Cr	Fe	Nb	Ni	V
Md (eV)	1.142	0.858	2.117	0.717	1.543

Acknowledgements Authors would like to thank Dr. G. Amarendra, Director, Metallurgy and Materials Group, and Dr. A. K. Bhaduri, Director, Indira Gandhi Centre for Atomic Research for their sustained support and encouragement in the pursuit of this work. Mr. Saikumaran expresses his deep sense of gratitude to HBNI for funding this project. The authors also thank UGC-DAE consortium for SEM facilities, Dr. N. V. Chandrasekar and Mr. Meenakshi sundaram for their help in alloy melting, Dr. S. Kalavathy and Mr. Irshad. K. Abbas for the XRD experiments.

Compliance with Ethical Standards

Data Availability The raw/processed data required to reproduce these findings cannot be shared at this time as the data also forms part of an ongoing study.

References

1. Yeh J W, Chen S K, Lin S J, Gan J Y, Chin T S, Shun T T, Tsau C H, and Chang S Y, *Adv Eng Mater* **6** (2004) 299.
2. Murty B S, Yeh J-W, and Ranganathan S, *High-entropy Alloys*, Butterworth-Heinemann, Oxford (2014).
3. Zhang Y, Zuo T T, Tang Z, Gao M C, Dahmen K A, Liaw P K, and Lu Z P, *Prog Mater Sci*, **61** (2014) 1.
4. Tsai M-H, and Yeh J-W, *Mater Res Lett* **2** (2014) 107.
5. Yeh J-W, *Jom* **65** (2013) 1759.
6. Huang Y-S, *Recent Patents Mater Sci* **2** (2009) 154.
7. Cantor B, Chang I, Knight P, and Vincent A, *Mater Sci Eng A* **375** (2004) 213.
8. Lin C-M, Tsai H-L, and Bor H-Y, *Intermetallics* **18** (2010) 1244.
9. Ng C, Guo S, Luan J, Shi S, and Liu CT, *Intermetallics* **31** (2012) 165.
10. Ke G-Y, Chen S-K, Hsu T, and Yeh J-W, *Annales de chimie Lavoisier* **31** (2006) 669.
11. Guo S, Ng C, and Liu CT, *J Alloy Compd* **557** (2013) 77.
12. Zhou Y, Zhang Y, Wang F, Wang Y, and Chen G, *J Alloy Compd* **466** (2008) 201.
13. Zhou Y, Zhang Y, Wang Y, and Chen G, *Mater Sci Eng A* **454** (2007) 260.
14. Zhou Y, Zhang Y, Wang F, and Chen G, *Appl Phys Lett* **92** (2008) 241917.
15. Wu Y, Cai Y, Wang T, Si J, Zhu J, Wang Y, and Hui X, *Mater Lett* **130** (2014) 277.
16. Wang Z, Guo S, and Liu C T, *JOM* **66** (2014) 1966.
17. Hsu C-Y, Juan C-C, Wang W-R, Sheu T-S, Yeh J-W, and Chen S-K, *Mater Sci Eng A* **528** (2011) 3581.
18. Juan C-C, Hsu C-Y, Tsai C-W, Wang W-R, Sheu T-S, Yeh J-W, and Chen S-K, *Intermetallics* **32** (2013) 401.
19. Jiang H, Jiang L, Han K, Lu Y, Wang T, Cao Z, and Li T, *J Mater Eng Perform* **24** (2015) 4594.
20. Tsai M-H, Yuan H, Cheng G, Xu W, Jian W W, Chuang M-H, Juan C-C, Yeh A-C, Lin S-J, and Zhu Y, *Intermetallics* **33** (2013) 81.
21. Tsai C-W, Chen Y-L, Tsai M-H, Yeh J-W, Shun T-T, and Chen S-K *J Alloy Compd* **486** (2009) 427.
22. Tsai M-H, Yuan H, Cheng G, Xu W, Tsai K-Y, Tsai C-W, Jian W W, Juan C-C, Shen W-J, and Chuang M-H, *Intermetallics* **32** (2013) 329.

23. Xu X, Liu P, Guo S, Hirata A, Fujita T, Nieh T, Liu C, and Chen M, *Acta Mater* **84** (2015) 145.
24. Furtek A, in *Book of Abstracts and Proc. 7th Int. Conf. Nuclear Option in Countries with Small and Medium Electricity Grids*, (eds) Cavlina N, Pevec D, Bajs T, Croatian Nuclear Society, Croatia (2008) 19.
25. Murty K, and Charit I, *J Nucl Mater* **383** (2008) 189.
26. Yvon P, and Carré F, *J Nucl Mater* **385** (2009) 217.
27. Yvon P, *Structural Materials for Generation IV Nuclear Reactors*, Woodhead Publishing, Cambridge, 2016.
28. Avilov A, Kuligin K, Nicolopoulos S, Nickolskiy M, Boulahya K, Portillo J, Lepeshov G, Sobolev B, Collette JP, Martin N, and Robins AC, *Ultramicroscopy* **107** (2007) 431.
29. Kolb U, Gorelik T, Kübel C, Otten M, and Hubert D, *Ultramicroscopy* **107** (2007) 507.
30. Kolb U, Gorelik T, and Otten M, *Ultramicroscopy* **108** (2008) 763.
31. Sheng G, and Liu CT, *Prog Nat Sci Mater Int* **21** (2011) 433.
32. Yang X, and Zhang Y, *Mater Chem Phys* **132** (2012) 233.
33. Zhang Y, Zhou Y J, Lin J P, Chen G L, and Liaw P K, *Adv Eng Mater* **10** (2008) 534.
34. Mohanty S, Maity T, Mukhopadhyay S, Sarkar S, Gurao N, Bhowmick S, and Biswas K, *Mater Sci Eng A* **679** (2017) 299.
35. Mridha S, Samal S, Khan P Y, and Biswas K, *Metallurg Mater Trans A* **44** (2013) 4532.
36. Mohanty S, Gurao N, and Biswas K, *Mater Sci Eng A* **617** (2014) 211.
37. Sonkusare R, Divya Janani P, Gurao N, Sarkar S, Sen S, and Pradeep K, *Mater Chem Phys* **210** (2017) 269.
38. Takeuchi A, and Inoue A, *Mater Trans* **46** (2005) 2817.
39. Mehrer H (ed), *Landolt-Börnstein numerical data and functional relationships in science and technology*, Springer-Verlag, Berlin, Heidelberg, Group III, **26** (1990) p 47.
40. Morinaga M, Yukawa N, Adachi H, and Ezaki H, *Superalloys* **1984** (1984) 523.
41. Lu Y, Dong Y, Jiang L, Wang T, Li T, Zhang Y *Entropy* **17** (2015) 2355.
42. Zhang Y, Yang X, and Liaw P, *Jom* **64** (2012) 830.
43. He F, Wang Z, Cheng P, Wang Q, Li J, Dang Y, Wang J, and Liu C, *J Alloys Compd* **656** (2016) 284.
44. Jiang L, Lu Y, Wu W, Cao Z, and Li T, *J Mater Sci Technol* **32** (2016) 245.